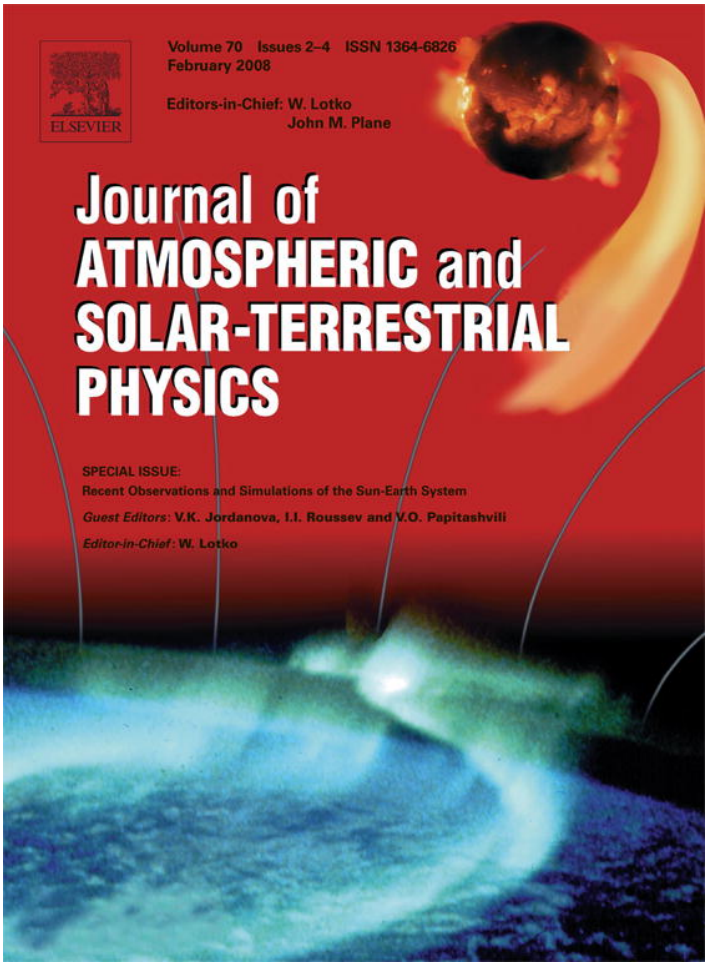

ELSEVIER

Journal of Atmospheric and Solar-Terrestrial Physics 70 (2008) 371–376

Journal of ATMOSPHERIC AND SOLAR-TERRESTRIAL PHYSICS

www.elsevier.com/locate/jastp

Tenuous solar winds: Insights on solar wind–magnetosphere interactions

C.J. Farrugia[a,*], F.T. Gratton[b], V.K. Jordanova[c], H. Matsui[a], S. Mühlbachler[d], R.B. Torbert[a], K.W. Ogilvie[e], H.J. Singer[f]

[a]*Space Science Center, University of New Hampshire, Durham, NH, USA*
[b]*INFIP, CONICET–FCEyN/UBA, Buenos Aires, Argentina*
[c]*Los Alamos National Lab, Los Alamos, NM, USA*
[d]*Max-Planck Institut fuer Sonnensystemforschung, Kathlenburg, Lindau, Germany*
[e]*NASA Goddard Space Flight Center, Greenbelt, MD, USA*
[f]*NOAA Space Environment Center, Boulder, CO, USA*

Accepted 27 July 2007
Available online 1 October 2007

Abstract

During solar cycle 23 quasi-dropouts of the solar wind (density $<1\,\mathrm{cm}^{-3}$) were observed. These tenuous winds allow us to probe properties of the magnetosphere and its coupling to the solar wind which would otherwise be obscured by the effect of high density. We focus on five areas which provided new insights into the response of geospace to solar wind variations: (i) the magnetospheric magnetic configuration; (ii) the polar rain; (iii) dayside flux erosion; (iv) magnetosheath waves; and (v) ring current constants. We find: (i) the geostationary field had dipolar strength and was inclined by $\leqslant 5^{\circ}$ to the dipolar direction; (ii) the solar wind strahl, and consequently the polar rain, were intensified; (iii) the depression of the geostationary field (ΔB_{GS}) due to dayside flux erosion could be measured and was related to IMF B_z by $\Delta B_{GS} = -2.8 + 2.3B_z$ (nT); (iv) right-hand electromagnetic ion cyclotron waves were excited alone in the magnetosheath and were generated directly from the temperature anisotropy of the solar wind; (v) ring and magnetopause currents decreased to asymptotic values of 5 and 3 nT, respectively, which are substantially smaller than quiet-time values obtained from statistics.

Keywords: Low density solar wind; Dayside erosion; Quiet-time ring current constants; Magnetosheath waves

1. Introduction

The solar wind exhibits occasional partial dropouts of long duration when the density decreases below $1\,\mathrm{cm}^{-3}$. Their frequency tends to increase around solar activity maximum (Ogilvie et al., 2000; Richardson et al., 2001). Many were found to be due to ICMEs and corotating interaction regions. When the magnetosphere interacts with tenuous solar winds, properties of the coupling and of the magnetosphere/magnetosheath system which would otherwise not be evident can be isolated and studied. We discuss five aspects: (i) The magnetospheric magnetic configuration; (ii) electron

*Corresponding author. Tel.: +1 603 862 4596; fax: +1 603 862 0311.
E-mail address: charlie.farrugia@unh.edu (C.J. Farrugia).

1364-6826/$ - see front matter © 2007 Elsevier Ltd. All rights reserved.
doi:10.1016/j.jastp.2007.08.032

precipitation into the polar caps; (iii) dayside magnetosphere erosion; (iv) magnetosheath waves; and (v) geomagnetic disturbances of quiet-time current systems. The period considered is May 10–12, 1999, where May 11 is known as "*The day the solar wind almost disappeared*".

2. Observations

2.1. The interplanetary medium

Interplanetary (IP) plasma data acquired by Wind are shown in Fig. 1: proton density, temperature, bulk speed, dynamic pressure, and magnetosonic Mach number. From 12 UT, May 10–16 UT, May 11, the density N_{sw} decreases quasi-exponentially, reaching lowest values of $\sim 0.3\,cm^{-3}$ (dynamic pressure, $P_{dyn} \approx 0.07$ nPa). The magnetosonic Mach number M_{ms} is close to unity in the second half of May 11, implying a very weak, or absent, bow shock.

We performed a minimum variance analysis (Sonnerup and Cahill, 1967) over the interval 9 UT, May 10–4 UT, May 12, shown in Fig. 2. A reliable normal was found (ratio of intermediate-to-minimum eigenvalues = 4.5) with a normal component ($B_k \equiv B_n$) $\approx$ 0 nT. Further, from the direction of the normal, we find that the IP structure associated with the density decrease was in this case a planar IP structure containing the Parker spiral

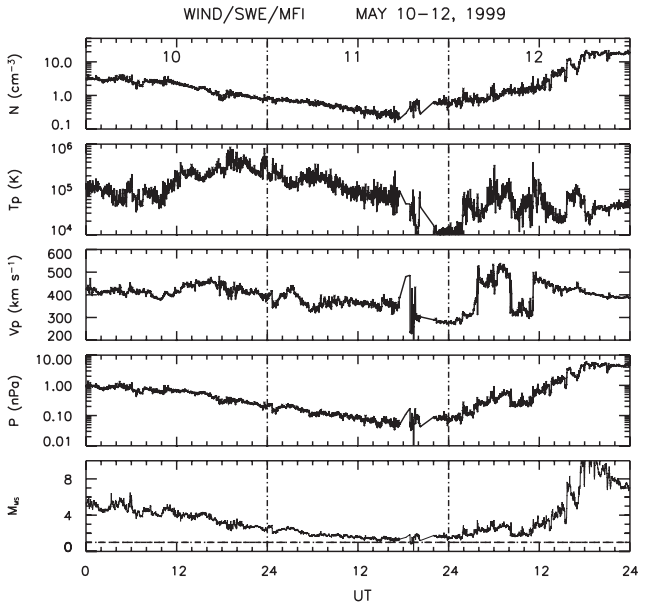

Fig. 1. Plasma data from spacecraft Wind for May 10–May 12, 1999: proton density, temperature, bulk speed, dynamic pressure, and magnetosonic Mach number.

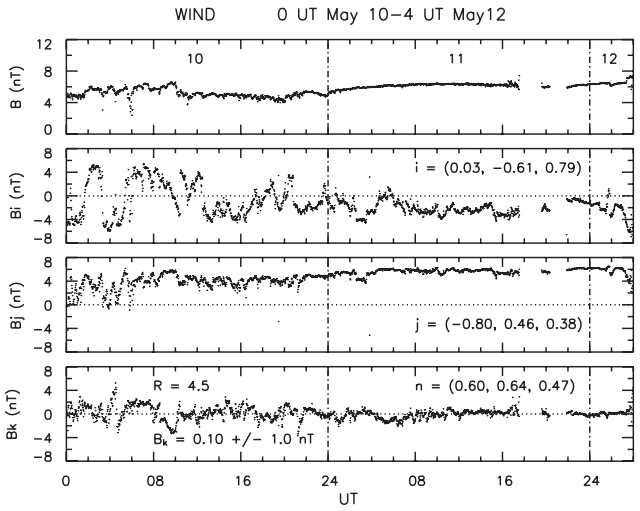

Fig. 2. The IMF plotted in minimum variance coordinates (i, j, $k \equiv n$). The unit vectors in GSM coordinates are noted in panels 2–4.

(Nakagawa et al., 1989; Farrugia et al., 2005). On May 11, 1999, the magnetic field is tilted antisunwards (IMF $B_x < 0$), and northward (average clock angle $\approx 45^\circ$).

2.2. The magnetospheric configuration

Fig. 3 shows with black traces the total geomagnetic field strength B measured at GOES 8, and its inclination θ to a dipolar field. The red trace gives the dipolar field strength along the spacecraft track. Open circles mark local magnetic noon. The diurnal variation of B becomes attenuated until, from 12 UT, May 11–4 UT, May 12 (purple bar) the geomagnetic field matches the dipole in both strength and direction (to within 5°). The dipolarization found at equatorial heights (Farrugia et al., 2000) was matched by a dipolarization at high latitudes (Le et al., 2000).

2.3. The polar rain

In Fairfield and Scudder (1985) it was proposed that the solar wind *strahl*, i.e. the field-aligned electron beam carrying the heat flux from the Sun, ought to be more intense in the preferred hemisphere (the northern one for, as here, an antisunward tilted IMF) if N_{sw} is low because under these circumstances pitch angle broadening by Coulomb collisions is reduced or eliminated. Thus, by conserving the magnetic moment ($\sim V_\perp^2/B$), the strahl remains highly collimated. The expectation is thus for intense strahls in the northern hemisphere.

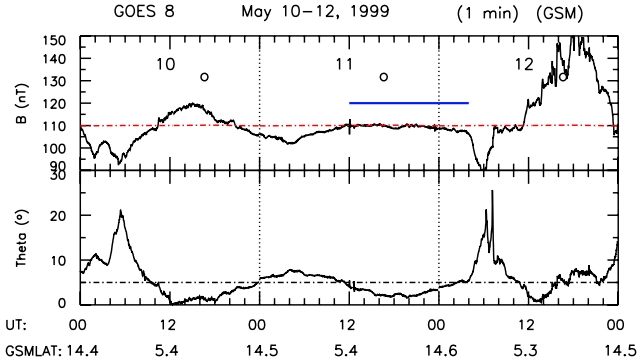

Fig. 3. The geomagnetic field, B, at GOES 8 for May 10–12: strength and inclination to a dipolar field. During the interval delimited by the horizontal purple bar, the field strength is that of the dipole (red trace) inclined at $\leqslant 5^\circ$ to the dipole.

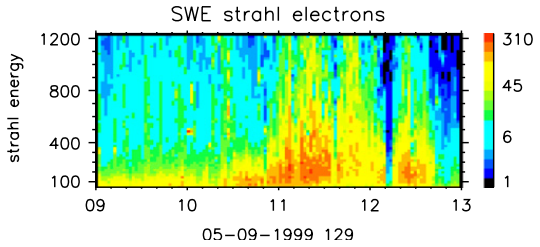

Fig. 4. Wind observations of a dramatic intensification of strahl electrons on May 11, 1999.

The May 1999 event corroborated this idea. Ogilvie et al. (2000) investigated strahl examples in low N_{sw} solar winds. They found that its angular width was $<3.5^\circ$. Fig. 4 shows Wind/SWE (Ogilvie, 1995) measurements of the strahl for May 9–12, 1999. The beam intensifies from late May 10–mid May 12 during the density decrease. It is most intense on May 11, during the lowest N_{sw} recorded. Analyzing the phase space density of the strahl, coronal electron temperatures of 100–150 eV were deduced (Ogilvie et al., 2000).

Fig. 5 shows Polar/Hydra (Scudder et al., 1995) observations from 13 UT, May 11–01 UT, May 12. Differential ion and electron energy fluxes, corrected for effects of spacecraft potential, are plotted against time, with intensities given by the respective scales on the right. At the bottom are shown the invariant latitude (ILT), magnetic local time (MLT), and radial distance of the spacecraft.

Polar made a long overflight of the northern polar cap. Very intense e^- fluxes are recorded. These may be contrasted with typical polar rain fluxes, when significant values lie in the few $\times 10^2$ eV range only. The extreme inter-hemisphere asymmetry

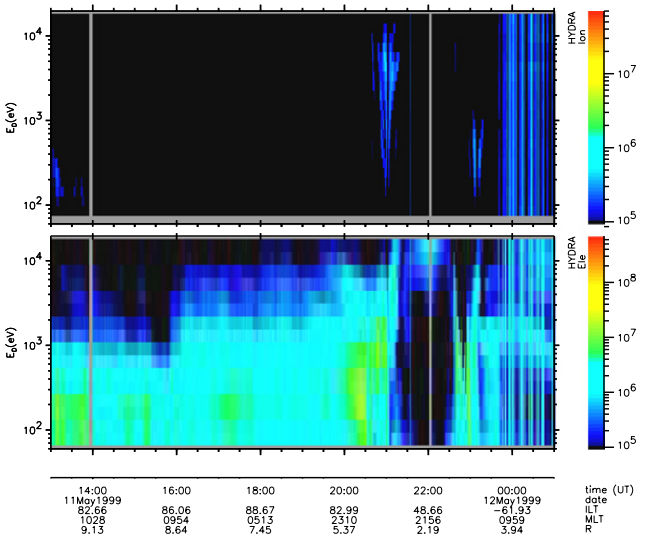

Fig. 5. Differential energy fluxes of ions and e^- during Polar's pass over the northern polar cap. Values in the southern polar cap may be (just) seen at 22:30 UT.

may be seen by comparing with values over the southern polar cap, overflown by Polar at ~22 : 30 UT soon after it passed perigee.

2.4. Dayside magnetosphere erosion

Interestingly, low N_{sw} intervals have been used to infer the dependence of dayside erosion on IMF B_z. The method is indirect and is based on the decrease in the geostationary field strength B_{GS} caused by erosion (Sibeck, 1994). Two factors affect B_{GS}: the solar wind P_{dyn}, tending to compress it, and dayside erosion, tending to depress it. By far the stronger effect is that of P_{dyn}. However, low N_{sw} winds can reduce P_{dyn} to the extent that the decrease of B_{GS} due to erosion becomes the larger effect.

A study of low-N_{sw} solar winds from this point of view was undertaken by Farrugia et al. (2001). May 11, 1999 was chosen as reference since (i) it had the lowest P_{dyn} of the whole set; and (ii) IMF was northward pointing. Thus the geostationary field was being, to a good approximation, neither compressed nor eroded. For the other events IMF $B_z<0$ nT.

A particularly trenchant example occurred during Earth passage of the February 10, 1997 magnetic cloud with its strongly southward field. Fig. 6 shows Wind measurements of P_{dyn} and IMF B_z in the top two panels, plotted with appropriate propagation delays. GOES 8 was making measurements near noon (10–12 MLT; panel 3). The Earth's field is more compressed on February 10, 1997 (~0.4 vesus ~0.07 nPa); yet

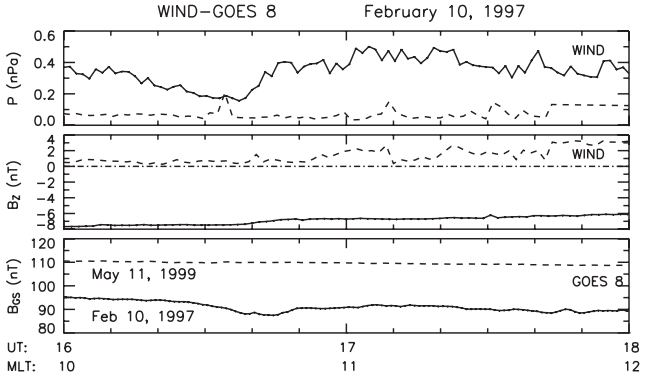

Fig. 6. Wind and GOES 8 observations on February 10, 1997 (solid trace) and May 11, 1999 (dashed trace): solar wind dynamic pressure, IMF B_z and the strength of the geostationary field.

B_{GS} is lower (i.e. less than the dipolar value). This is a result of erosion of the dayside magnetosphere caused by the cloud $B_z<0$. After correcting for the effect of P_{dyn}, we obtain ΔB_{GS} as a function of IMF B_z. The result is ΔB_{GS} (nT) $= -2.8 + 2.3B_z$ (nT) with a correlation coefficient of 0.9 (six events).

2.5. Plasma waves in the magnetosheath

The solar wind Alfven Mach number, M_A, plays a key role in the structure of the magnetosheath. Low values imply a strong control by the IMF, leading to a wide plasma depletion layer, PDL. Quantity M_A may be expressed as $M_A^2 = \mu_0 P_{dyn}/B^2$. Thus for constant B (expected for low N_{sw}, Fig. 1), low P_{dyn} implies low M_A and so a wide PDL. The major wave mode in the PDL is electromagnetic ion cyclotron waves (EICW), driven by the proton temperature anisotropy $A_p = T_\perp/T_\parallel - 1$ (e.g. Anderson, 1995). The EICWs are found to consist of a mixture of right (RH)- and left-handed (LH) polarities. The solar wind at 1 AU has typically $A_p<0$. Passage through the bow shock raises $T_\perp$, and A_p becomes positive. When $A_p>0$, only the LH EICWs are excited, but the RH EICWs may still appear in the recorded spectrum as by-products of the LH EICWs. This is partly because of possible large Doppler-shifts of LH EICWs, and partly because RH EICWs can be generated from LH EICWs by nonlinear wave interactions. These, therefore, may be called "daughters" of the LH EICWs. According to the linear wave theory, RH EICWs can be excited by a negative A_p provided the plasma β_p is not too small, but at the same time $A_p<0$ inhibits the growth of LH EICWs. Thus, the RH EICWs are observed sometimes together with LH ICWs and at other times alone, and we show experimentally that this is well correlated with the periods of positive and negative A_p, respectively.

The weak bow shock on May 11, 1999 exposed the magnetosheath plasma directly to the A_p of the solar wind, which was negative ($T_\parallel > T_\perp$), according to the measurements of Wind (Farrugia et al., 2005). In this case, if there are RH EICWs they would have been generated directly from the negative A_p of the solar wind (see below).

Geotail was traversing the duskside magnetosheath. Fig. 7 shows power spectral densities (PSD) for 06–18 UT, May 11, divided into two intervals. Plotted are the PSD transverse to (LH polarized, B_L, and RH polarized, B_R), and along, the magnetic field (compressional, B_z), calculated in field-aligned coordinates. The number of points in each fast Fourier transform (FFT) is 1024, and the resolution of the magnetometer data is 16 Hz. We slide the FFT window for every 512 points to calculate the average spectra. In the first interval, LH components are dominant and peak around ~0.24 Hz, while RH components are the dominant, though weaker, wave emission during the second interval, namely, that when the bow shock is very weak or absent after 12 UT, May 11 (Fig. 1). (Compressional power is not significant in either interval, indicating that no mirror mode waves are excited in this low-β plasma environment.) This is a direct confirmation of theoretical expectations and the only reported case of RH EICW in the magnetosheath occurring in the absence of the LH EICWs that we are aware of.

The theory behind the excitation of RH polarized waves by $T_\parallel > T_\perp$ ($A_p<0$) can be briefly summarized as follows. Fig. 8 shows a plot of kV_A/Ω_C versus ω/Ω_C (Ω_C = proton gyrofrequency). The solid blue curve represents the dispersion relation of EICW RH polarized waves. Close to $\omega = 0$, the phase velocity coincides with the Alfven velocity V_A (dotted blue line). The diagram is for (parallel plasma beta) $\beta_\parallel < 1$, which implies a thermal speed, $v_{th} < V_A$, the Alfven speed.

Only those protons which satisfy the anomalous resonant condition $\omega - kv_\parallel = -\Omega_C$ (straight lines passing through $\omega/\Omega_C = -1$ and crossing the solid blue curve) can interact with the waves. Particles must move fast and overtake the wave, so that they can feel the electric field gyrating LH at the proton cyclotron frequency. Furthermore, for wave amplification the intersection point must satisfy the condition $\omega/\Omega_C \le |A_p|/(1 - |A_p|)$. Above this critical

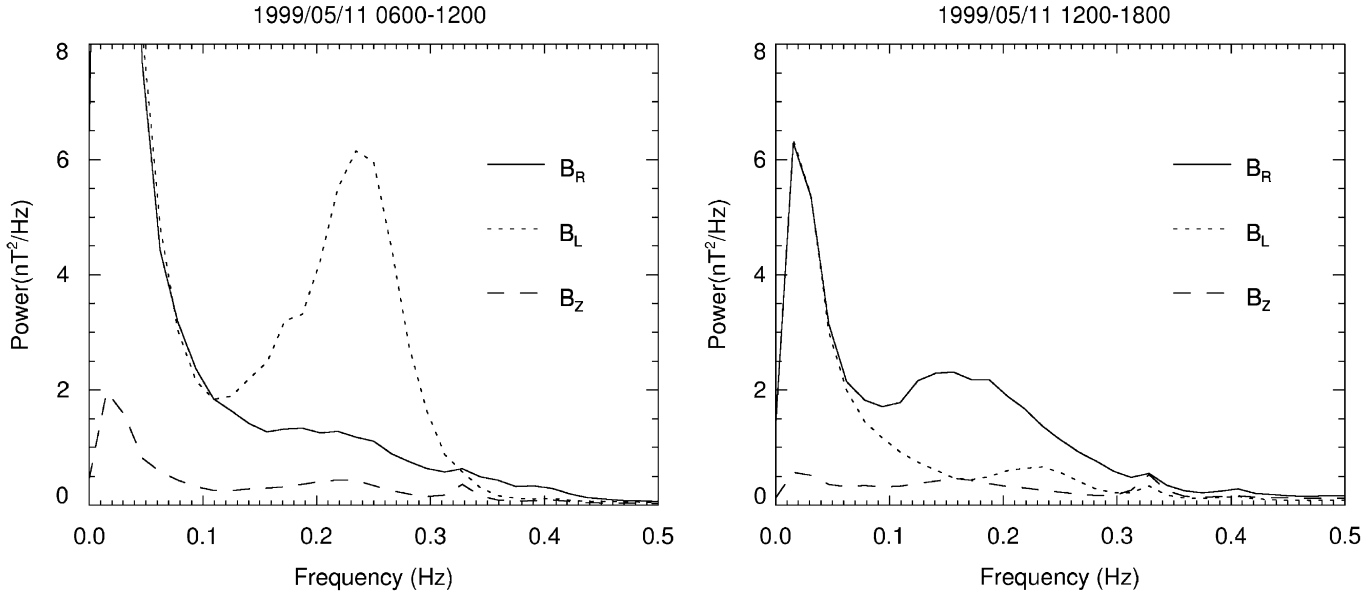

Fig. 7. For two time intervals on May 11, 1999, the figure shows power spectral densities transverse to (short dashed and solid lines), and along (long dashed line), the magnetic field calculated in field-aligned coordinates.

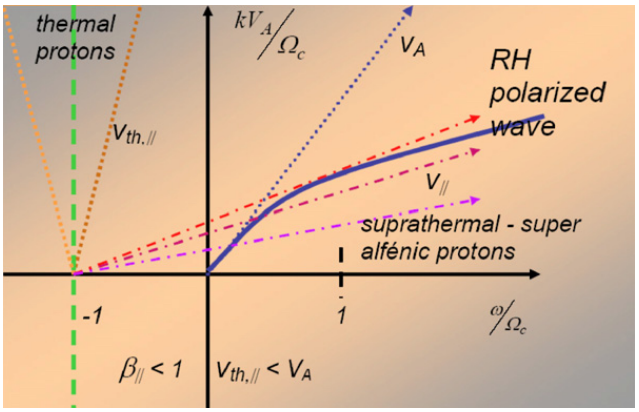

Fig. 8. Dispersion relation of RH EICWs (solid blue line) for $\beta_{\parallel} < 1$. Close to $\omega = 0$ the phase velocity is V_A (dotted blue line); all speeds are normalized with V_A. Straight (dotted) lines close to $\omega/\Omega_C = -1$ represent thermal protons $v_{th,\parallel} < V_A$. Straight (dotted) lines through $\omega/\Omega_C = -1$ that cross the dispersion relation represent instead protons that satisfy the anomalous resonant condition and interact with the waves.

frequency, absorption dominates over emission and no RH waves are produced.

The red dot-dashed lines correspond to protons moving with large velocities $v_{\parallel} > V_A$ (and $v_{th,\parallel}$). The lines around $\omega/\Omega_C = -1$ correspond instead to thermal protons. Ordinarily, only few protons of the bi-Maxwellian tail can resonate with the wave in conditions favorable to excitation, which explains the difficulty of observing first generation (as opposed to "daughter") RH polarized waves produced by negative A_p, as was instead the case of the event reported here.

2.6. Quiet-time ring current constants

Jordanova et al. (2001) used a kinetic drift-loss model (e.g. Jordanova et al., 1999) to simulate the global evolution of the ring current ions during May 10–11, 1999 and compare the effect of the magnetopause, ring, magnetotail and field-aligned currents on the Dst index. There is no consensus in the literature at present on these quiet-time Dst effects. The model calculates drifts of ring current ions in a time-dependent magnetospheric electric field (Volland, 1973; Stern, 1975; Maynard and Chen, 1975) and a dipolar geomagnetic field. As noted, the dipolarity assumption is very closely justified during these quiet conditions. Furthermore, from the small standard deviations of the Dst and the planetary Kp indices, the Kp-dependent Volland–Stern convection electric field should also be appropriate to high degree of accuracy. As shown in Fig. 9, the ground magnetic field disturbances due to the ring and magnetopause currents decrease quasi-monotonically on May 11, reaching limiting values of ~5 and ~3 nT, respectively. These values are substantially smaller than the ~20 nT quiet time values obtained in statistical studies. (But see Jorgensen et al., 2004 who obtained values for the quiet-ring current of 3.84 ± 4.33 nT, similar to ours.) Though only a case study, the particularly favorable

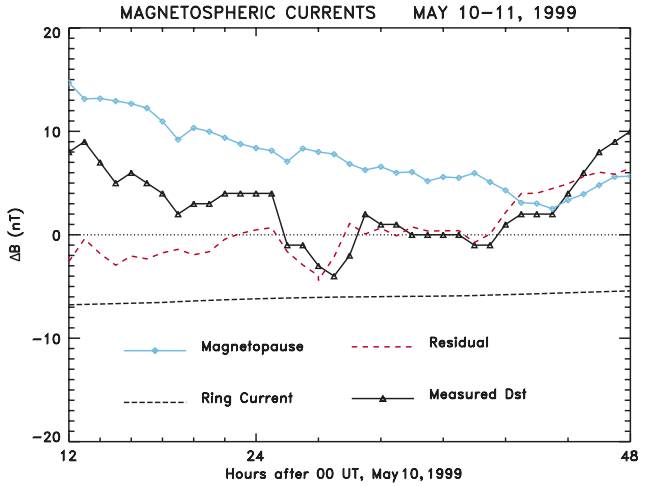

Fig. 9. The magnetic disturbances due to magnetopause, ring, magnetotail and field-aligned currents on the Dst index.

conditions for the simulation lend more weight to these results. Discrepancies with statistical studies may be due to the inclusion of moderately disturbed conditions (e.g. Kp$<2+$ versus Kp$=0+$ here) in the latter.

3. Conclusions

The following are some of the insights into solar wind–magnetosphere interactions gained from the effects elicited in the magnetosphere/magnetosheath by tenuous solar winds:

(i) The geomagnetic field becomes dipolar if IMF $B_z>0$ (small clock angle). (ii) If the clock angle is large, the geomagnetic field is less than dipolar, a signature of flux erosion from the dayside. (iii) With low P_{dyn} we can eliminate a major influence on B_{GS}, and enter a regime where the effect of erosion is (i) bigger and (ii) can be measured confidently as a function of IMF B_z. (iv) Using low P_{dyn} winds, we can determine quiet-time ring current constants using a magnetic field model (dipolar) which is employed anyway but whose use is justified in this case. These constants can then be used for modeling the ring current under all IP conditions. (v) One aspect of the Sun–Earth connection is highlighted: Coronal electrons precipitating into the polar caps are more intense because Coulomb scattering is reduced. (vi) The weakened bow shock exposes the magnetosheath plasma to the proton temperature anisotropy of the solar wind, which is typically negative. Under these conditions, EICWs of left-hand polarity are not excited, and those of right-hand polarity are generated directly from the temperature anisotropy of the solar wind. This is a further insight into MHD effects on the magnetosheath in as much as, under low dynamic pressure, the Alfven Mach number is also low.

Acknowledgments

We thank T. Nagai for the Geotail magnetometer data This work is supported in part by NASA Grants NNG05GC75G, NNG06GD41G, WIND-SWE and NAG5–13512 and MFI Analysis and STEREO grant to UNH. F.T.G. acknowledges supports of Argentinian grants, CONICET PIP5291, and UBACyT X291.

References

Anderson, B.J., 1995. In: Song, P., Sonnerup, B.U.O., Thomsen, M. (Eds.), Physics of the Magnetopause Geophysical Monograph, vol. 90, p. 269.
Fairfield, D.H., Scudder, J.D., 1985. Journal of Geophysical Research 90, 4055.
Farrugia, C.J., Singer, H.J., Evans, D.S., et al., 2000. Geophysical Research Letters 27, 3773.
Farrugia, C.J., Mühlbachler, S., Biernat, H.K., Torbert, R.B., 2001. Journal of Geophysical Research 106, 25,517.
Farrugia, C.J., Gratton, F.T., Gnavi, G., et al., 2005. Annales de Geophysique 23, 1317.
Jordanova, V., Farrugia, C.J., Quinn, J.M., et al., 1999. Journal of Geophysical Research 104, 429.
Jordanova, V., Farrugia, C.J., Fennell, J.F., Scudder, J.D., 2001. Journal of Geophysical Research 106, 25,529.
Jorgensen, A.M., Spence, H.E., Hughes, W.J., Singer, H.J., 2004. Journal of Geophysical Research 109, A12204 doi:10.1029/2003JA010090.
Le, G., Chi, P.J., Goedecke, W., et al., 2000. Geophysical Research Letters 27, 2165.
Maynard, N.C., Chen, A.J., 1975. Journal of Geophysical Research 80, 1009.
Nakagawa, T., Nishida, A., Saito, T., 1989. Journal of Geophysical Research 94, 11761.
Ogilvie, K.W., 1995. Space Science Reviews 71, 55.
Ogilvie, K.W., Fitzenreiter, R., Desch, M., 2000. Journal of Geophysical Research 105 (A12), 27,277.
Richardson, I.G., Berdichevsky, D., Desch, M.D., Farrugia, C.J., 2001. Geophysical Research Letters 27, 3761.
Scudder, J.D., et al., 1995. Space Science Reviews 71, 459.
Sibeck, D.G., 1994. Journal of Geophysical Research 99, 8513.
Sonnerup, B.U.O., Cahill, L.J., 1967. Journal of Geophysical Research 72, 171.
Stern, D.P., 1975. Journal of Geophysical Research 80, 595.
Volland, H., 1973. Journal of Geophysical Research 78, 171.